Table of contents

Supplementary figures

Supplementary Tables

Supplementary Figures

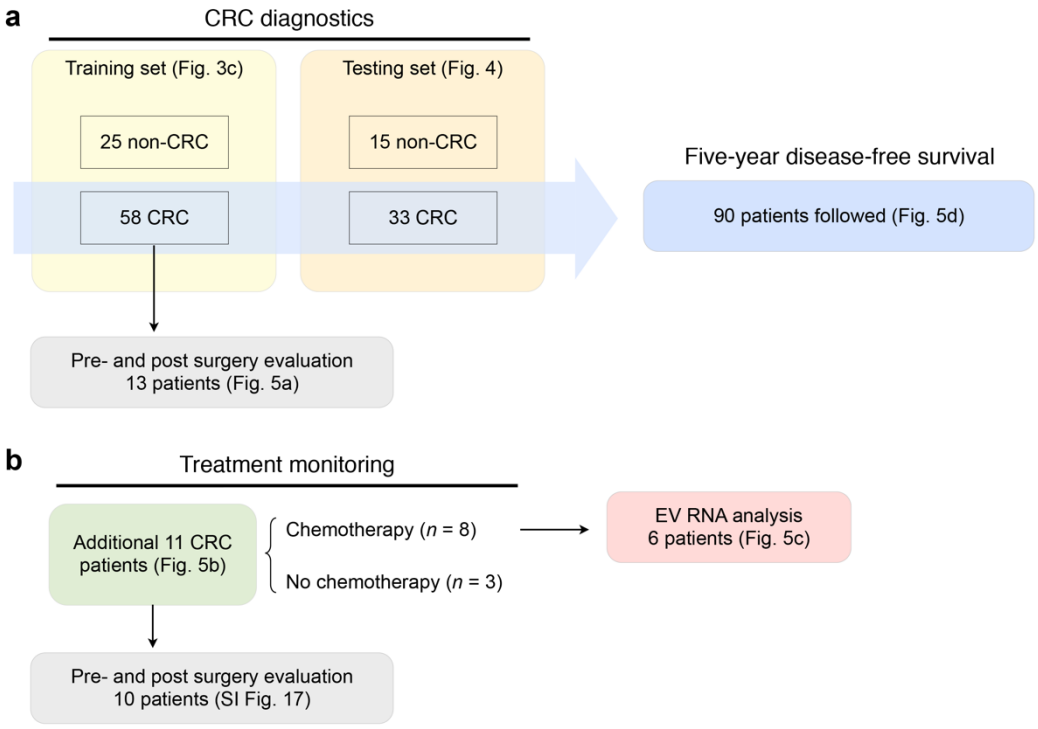

Figure S1 | Detailed study design. (a) Cohorts used for colorectal cancer (CRC) diagnostics (n = 131). These cohorts were used to determine diagnostic metrics for EV-based CRC detection and prognostics. The training set for CRC diagnostics had 25 non-CRC controls and 58 CRC patients, and the testing set had 15 non-CRC controls and 33 CRC patients. For 13 CRC patients in the training set, we obtained and analyzed blood samples before and after surgery. We followed 90 CRC patients up to 61 months to estimate 5-year disease-free survival. **(b)** Cohorts for treatment monitoring (n = 11). We recruited additional 11 CRC patients and serially analyzed their circulating EVs before surgery, within one week after surgery, and in six months after surgery. Of this cohort, eight patients received a standard chemotherapy after surgery. Samples from six treated patients were further subject to EV RNA profiling.

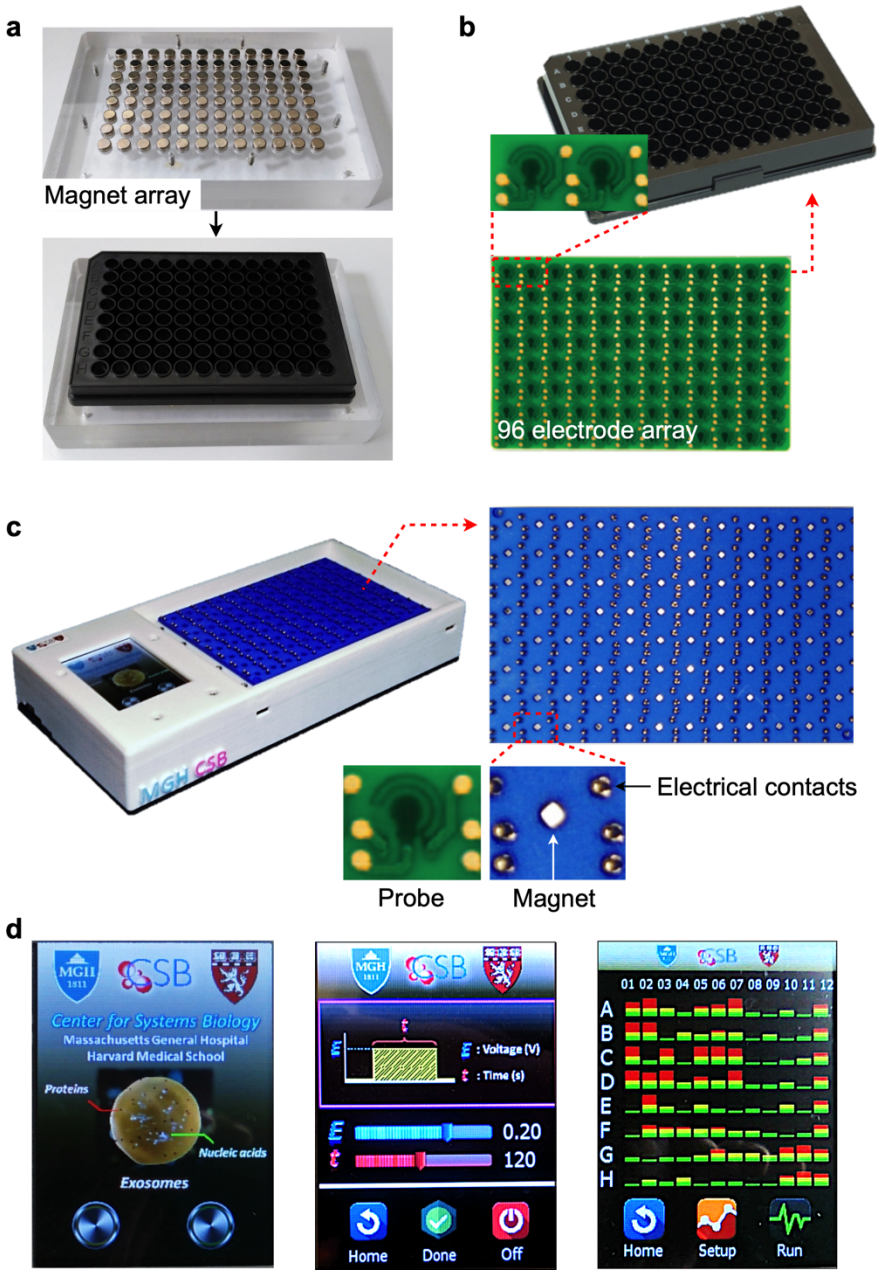

Figure S2 | HiMEX system for high throughput EV assays. (a) A custom-designed magnet array was used to batch-process samples during EV capture and labeling. **(b)** Electrodes used for the HiMEX assay. A 12 × 8 electrode array was attached on the back side of a bottomless-well plate. **(c)** The electrode array made electrical connections with the HiMEX reader through spring-loaded connectors. To concentrate EV-bound magnetic beads on the sensing surface, a small magnet was positioned at the center location of each electrode. **(d)** The HiMEX reader had a touchscreen interface for the system control. The setup screen (middle) presented controls to adjust the potential between working and reference electrodes and its duration. The result screen (right) displayed measured current values. The reader fast scanned all electrode, effectively carrying out parallel detection.

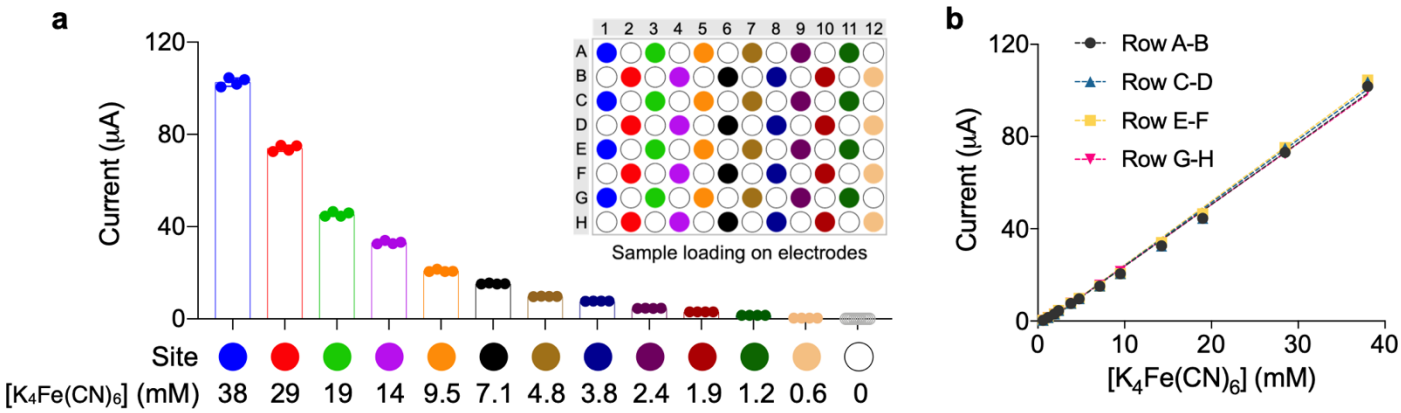

Figure S3 | HiMEX reproducibility test. (a) Standard samples with varying $K_4Fe(CN)_6$ concentrations were loaded into a 12 × 8 electrode array. The electrochemical reaction signals were measured by the HiMEX system in a parallel fashion. Each bar represents a mean value from technical replicates (n = 4). Inset shows the sample loading configuration. For a given $K_4Fe(CN)_6$ concentration, the measured currents at different sites were highly concordant. **(b)** Four titration curves, from one dilution sample in technical replicates, were generated by pairing two adjacent rows in the array. The slopes of four curves were statically identical (p = 0.42, one-way ANOVA, Tukey multiple comparisons test). Data points represent mean ± SEM from technical quadruplicates.

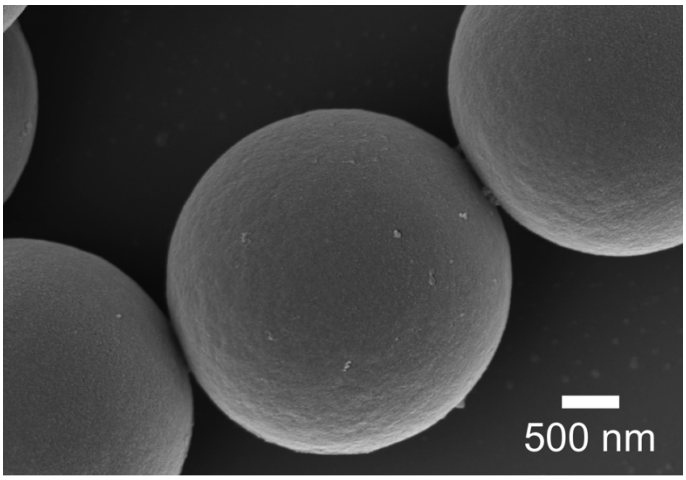

Figure S4 l EV capture with control beads. Microbeads, conjugated with IgG control antibodies, were incubated with EVs from HCT116 cell lines. Note the negligible EV binding on bead surface. A representative image from technical duplicates is shown.

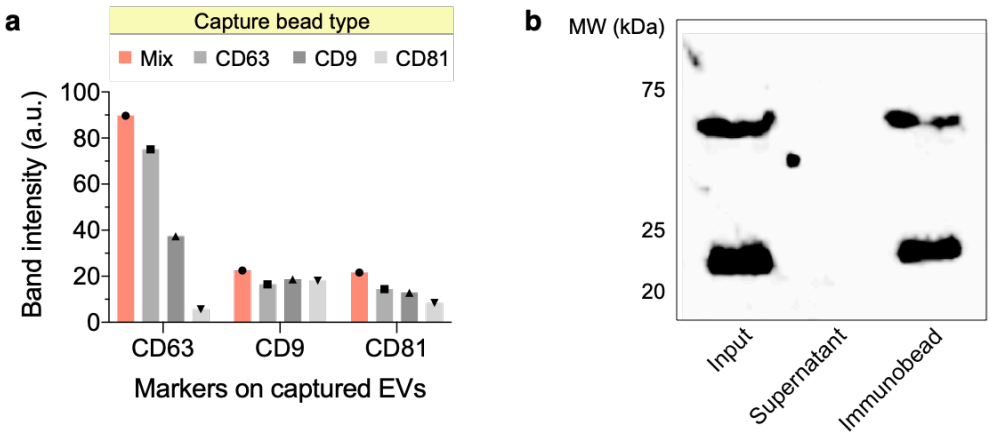

Figure S5 l Immunomagnetic EV capture. (a) The western blot image (n = 1) in **Fig. 2b** was digitized and band intensities of tetraspanins in pulled-down samples were quantified. Using a cocktail of beads (i.e., mixture of CD63, CD9, CD81 bead types) yielded higher EV levels of tetraspannins than using single bead types. **(b)** EV capture efficiency in plasma. EVs in human plasma were captured, and levels of CD63 were measured via western blotting. The capture efficiency, estimated from the band intensity, was about 82%.

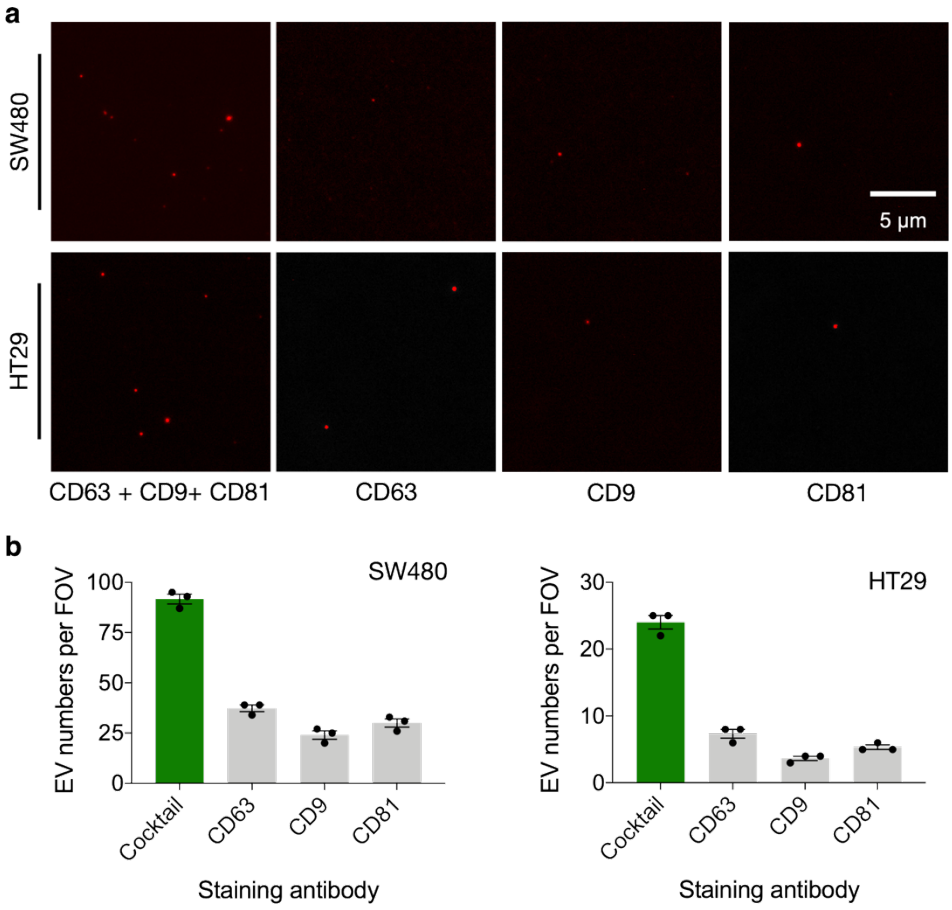

Figure S6 l Single EV imaging of tetraspanin markers. (a) EVs from CRC cell lines (SW480, HT29) were fluorescently labeled and imaged. The field-of-view (FOV) was 46.5 × 38.6 μm^2. Representative images from technical duplicates are shown. **(b)** Marker-positive EV numbers were counted. Using a cocktail of antibodies (CD63, CD9, CD81) resulted in the higher number of EVs stained than using single antibody types. Data are displayed as mean ± SEM from three FOVs.

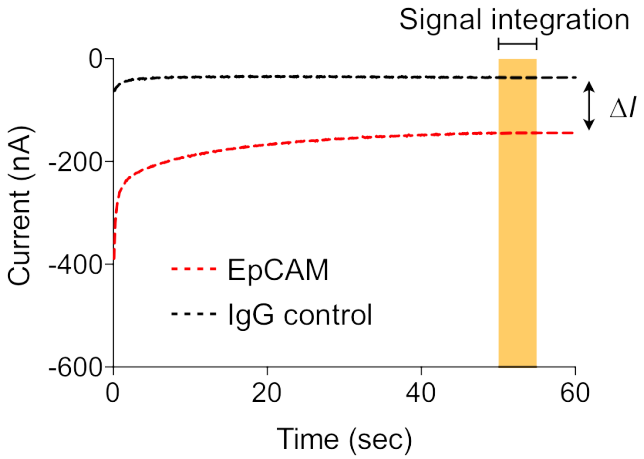

Figure S7 I Electrical current measurement with HiMEX. Electrochemical reactions were initiated with the application of the reduction potential between a working and a counter electrodes. The current level reached a plateau within 1 min. The average current (*I*) from 50 to 55 sec was obtained. The net current difference Δ*I* between a marker-specific and an IgG control currents were used as a representative value of a target protein marker.

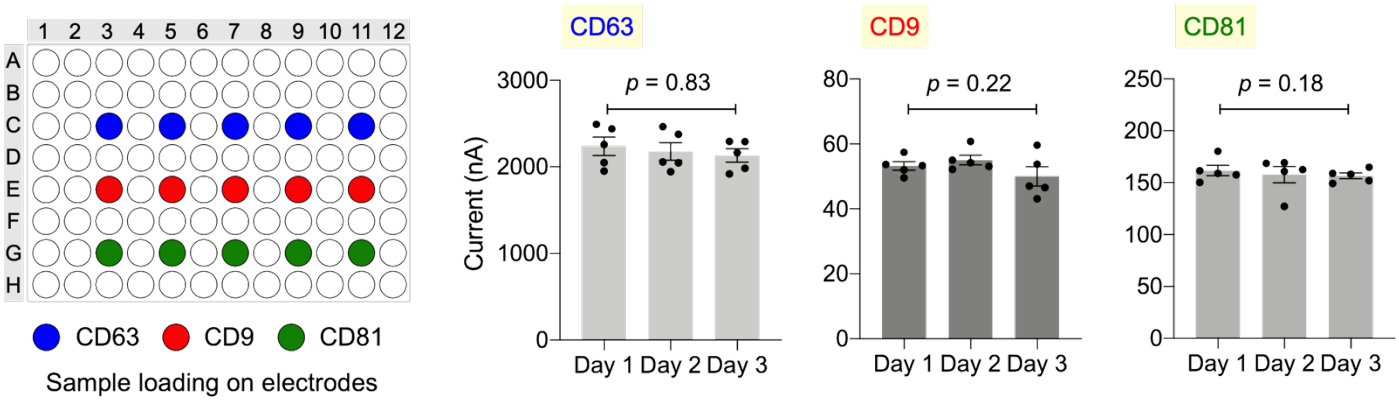

Figure S8 I Assay reproducibility. EV samples (~10^8 vesicles derived from SW480 cell line) were assessed by HiMEX on three different days. Samples were freshly prepared on the day of measurement. For a given marker, 5 different probes in the HiMEX array were used. Average marker expression was statistically identical among different day measurements (one-way ANOVA): $p = 0.73$ for CD63; $p = 0.26$ for CD9; $p = 0.80$ for CD81. Data are displayed as mean ± SEM.

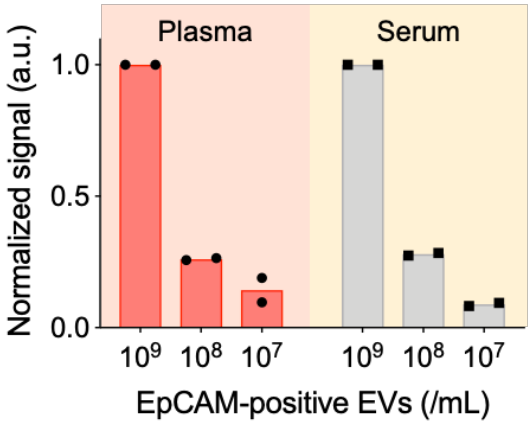

Figure S9 | Comparison of sample media. HiMEX signal from plasma and serum samples were compared. Samples were prepared by spiking known amount of EVs (derived from SW480 cell line) and EpCAM levels were measured by HiMEX. Note that both plasma and serum samples showed a similar trend. Each bar represents a mean value from duplicate measurements.

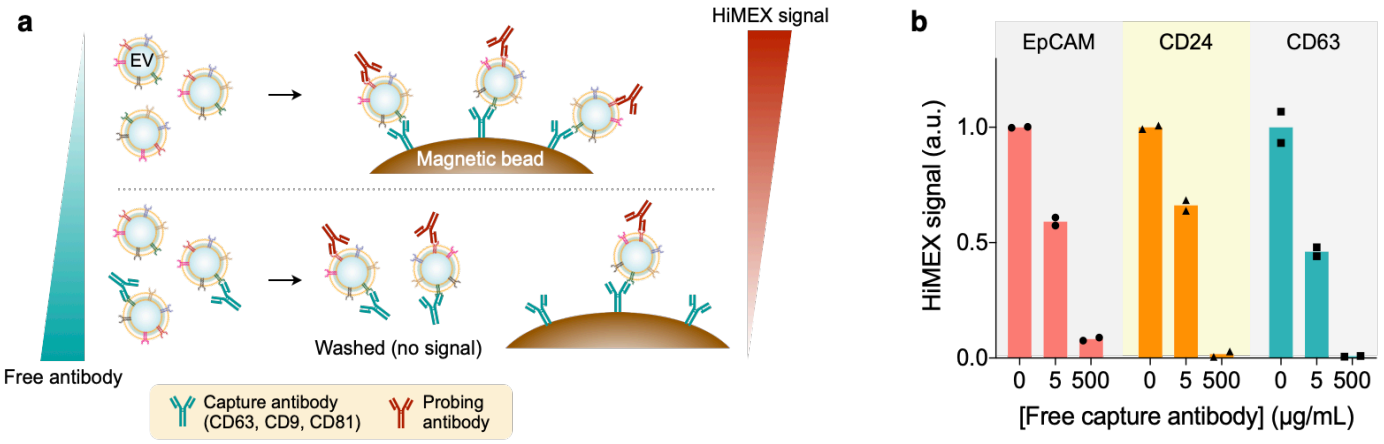

Figure S10 | Competition assay for EV capture. (a) Assay schematic. EVs (~10^9 vesicles) from a CRC cell line (SW480) were spiked in human plasma (1 mL) from a healthy donor. Immunomagnetic EV capture was performed in the presence of excess, free-floating capture antibodies (a cocktail of CD63, CD81, CD9 antibodies). Captured EVs were then labeled for HiMEX detection. **(b)** After competitive immunocapture, signal levels of EpCAM, CD24, and CD63 were measured by HiMEX. Note the signal decrease as higher concentrations of free antibodies are used. Each bar represents a mean value from duplicate measurements.

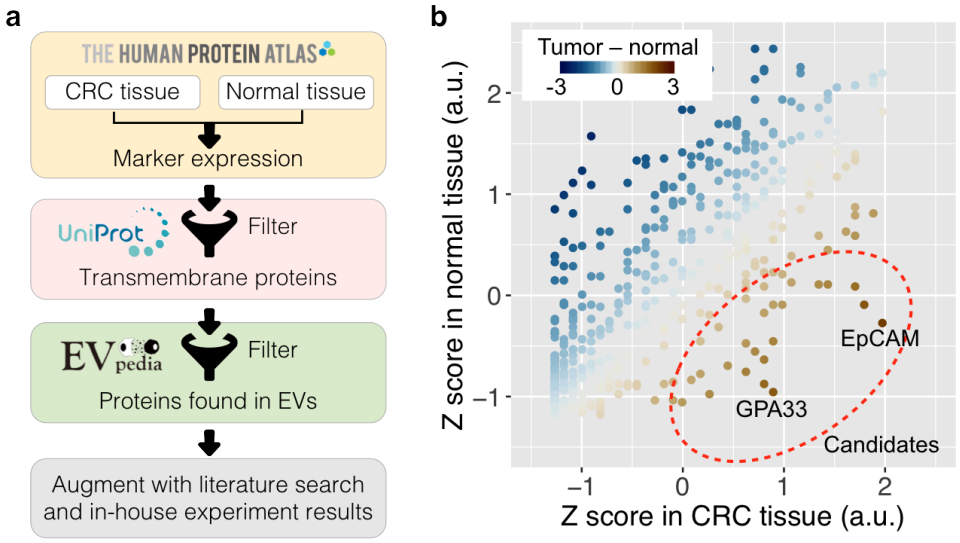

Figure S11 I Bioinformatic framework for the initial selection of CRC markers. (a) Selection algorithm. Protein expression profiles in CRC and normal tissues were retrieved from the Human Protein Atlas (HPA), and markers over-expressed in CRC tissues were identified. This list was narrowed down by cross-referencing the UniProt database to select proteins with transmembrane domains. Markers were further filtered for their presence in EVs according to the EVpedia database. The final list was augmented with markers from literature search and in-house profiling. **(b)** Protein markers identified through the analyses of HPA, UniProt, and EVpedia databases. For each tissue category (i.e., CRC, normal), the expression profile was standardized. Markers with high differential z-scores between CRC and normal tissues were chosen as potential candidates.

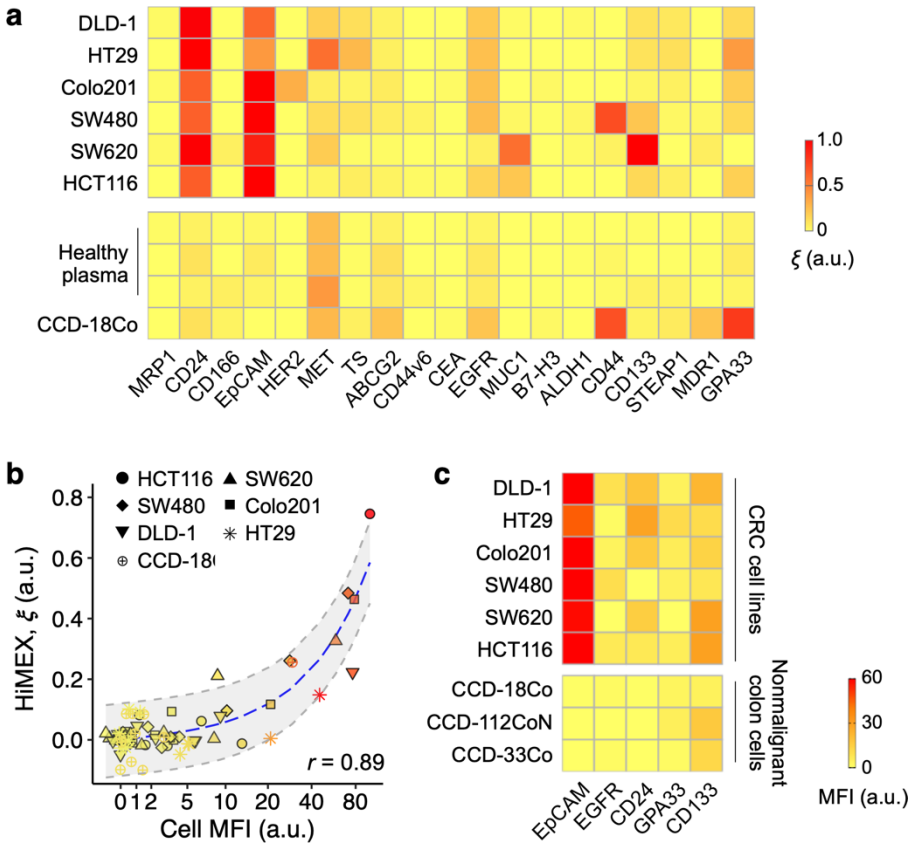

Figure S12 | Marker screening in cell lines. (a) Profiling EVs from CRC cells and normal control samples. A panel of CRC cell lines was used to encompass different CRC stages, per Dukes 'classification (SW480, Type B; DLD-1 and SW620, Type C; Colo201, Type D), and CRC resistant to irinotecan (HT29, HCT116). Normal control EVs were collected from healthy donor plasma samples and a human colon fibroblast cell line (CCD-18Co). Nineteen candidate markers, chosen from bioinformatic analyses and a literature search, were measured on EVs by HiMEX. **(b)** Protein profiles were highly correlated (Pearson correlation coefficient, $r = 0.89$) between EVs and their parent cells, supporting the use of EVs as a cellular surrogate. HiMEX data represent mean values from technical duplicates. Cells were analyzed via flow cytometry. Mean fluorescence intensity (MFI) were plotted in a pseudo-log scale for clarity. Data were plotted in log scales for clarity. The blue-dashed line indicates the best linear fit, and the shaded grey area 95% confidence band. **(c)** Five candidate markers (EpCAM, EGFR, CD24, GPA33, CD144) were further validated (via flow cytometry) on a panel of CRC and three non-malignant colon cell lines. Note the higher expression of these markers in CRC cell lines.

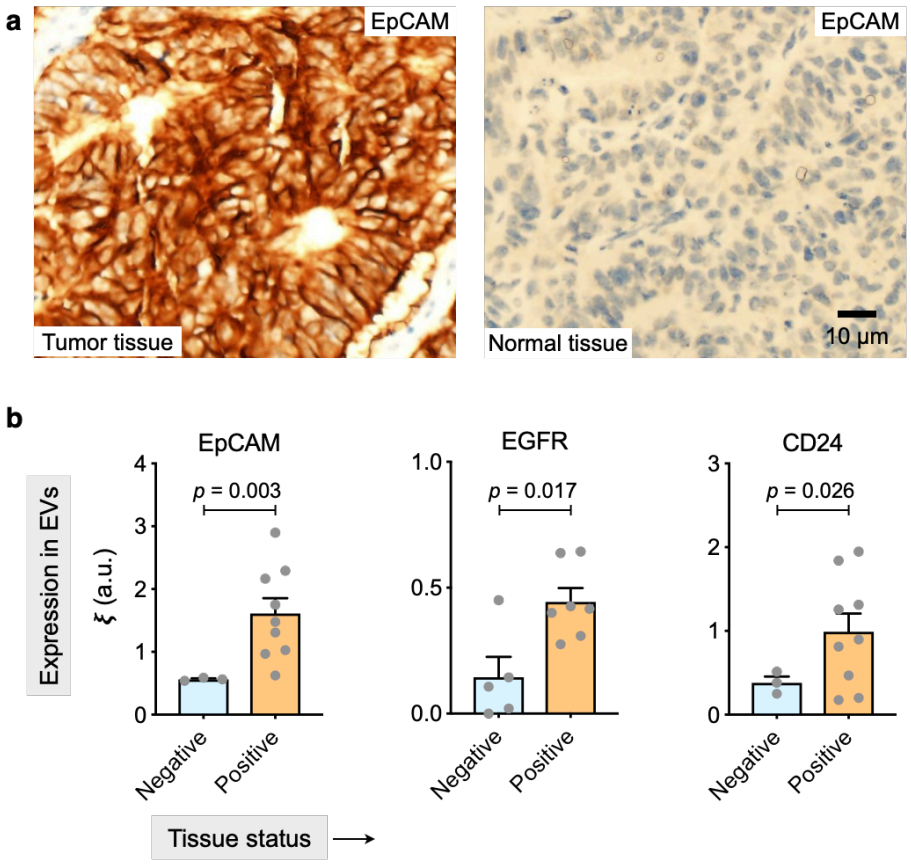

Figure S13 l Tissue and EV analyses from CRC patient samples. (a) Tumor and normal tissues were obtained from a same patient and immunostained. Representative images of EpCAM analyses from two patients are shown. Note the high expression of the marker in the tumor tissue. **(b)** CRC patients (n = 12) were dichotomized (negative vs. positive) according to the expression of a CRC marker in tumor tissue. The same marker was analyzed in patients 'plasma EVs. Overall, target markers were significantly elevated in EVs ($p < 0.05$; unpaired two-sided t-test) among patients with tissue-positive status. The bar graphs show mean ± SEM.

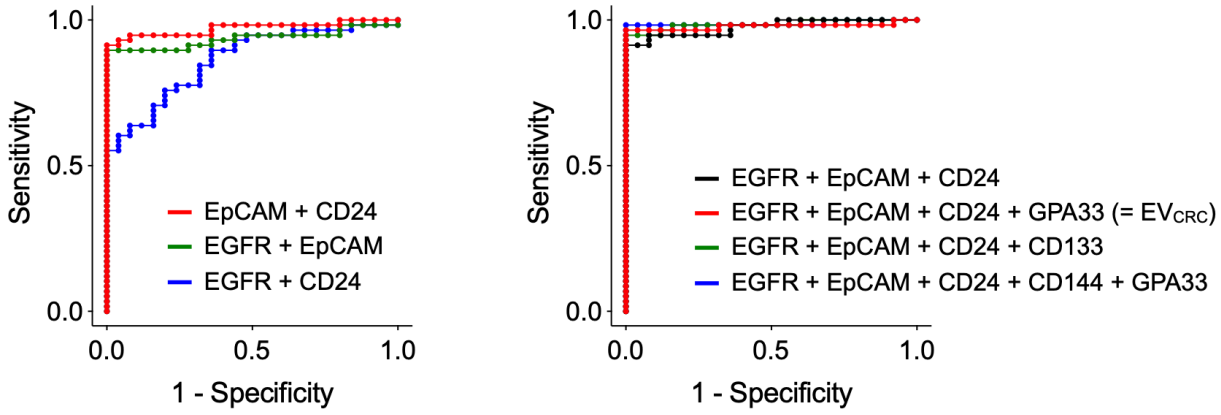

Figure S14 l Receiver operation characteristic (ROC) curves for multi-marker panels. For each panel, we used logistic regression to set the model of the weighted sums of EV markers. Training cohort was analyzed. ROC curves of two-marker panels (left) showed that EpCAM and CD24 are major contributors to diagnostic accuracy. Adding more markers incrementally improved the area under the curves (right).

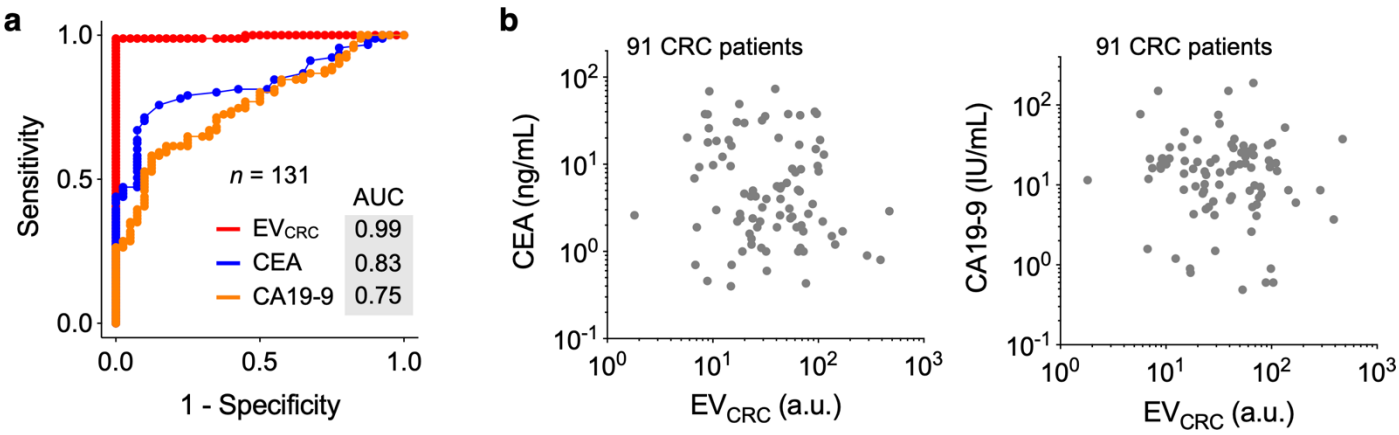

Figure S15 l Comparison of EV_{CRC} with conventional blood markers. (a) ROC curves were generated using the data from 91 CRC patients and 40 non-CRC controls. EV_{CRC} achieved higher AUC than conventional markers ($p < 10^{-4}$, EV_{CRC} *vs* CEA; $p < 10^{-6}$, EV_{CRC} *vs* CA19-9). **(b)** EV_{CRC} and CEA levels were compared among 91 CRC patients (left). No significant correlation ($p = 0.24$; two-sided Spearman nonparametric correlation test) was observed (Spearman $\rho_s = -0.12$). Similarly, EV_{CRC} had no significant ($p = 0.29$; two-sided Spearman nonparametric correlation test) correlation with CA19-9 (right; Spearman $\rho_s = -0.11$).

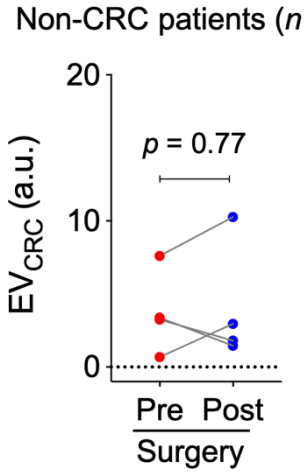

Figure S16 | EV monitoring before and after surgery. Non-CRC patient blood samples were analyzed before and after abdominal surgery ($n = 4$). EV_{CRC} values showed no significant changes ($p = 0.77$, paired two-sided *t*-tests). In contrast, the value decreased with CRC patients (**Fig. 5a**, main text). Each data point in the graph represents the mean value from technical duplicates.

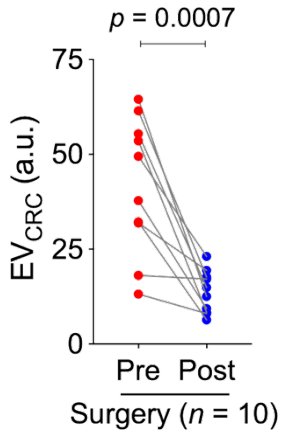

Figure S17 l Changes of EV_{CRC} before and after surgery. Additional cohort of 10 CRC patients from treatment monitoring was analyzed. EV_{CRC} values decreased in all patients after surgery (paired two-sided *t*-test, $p = 0.0007$).

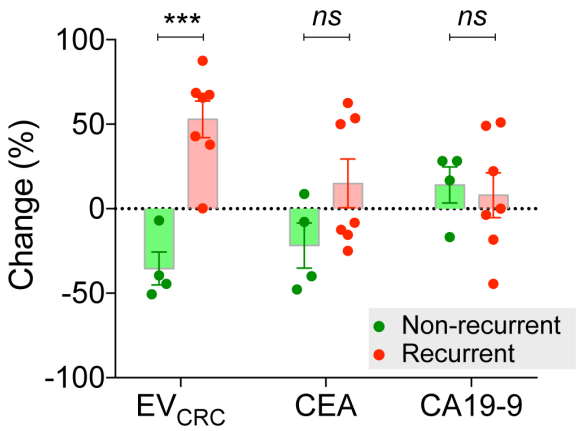

Figure S18 l Analyses on longitudinal CRC patient samples. Levels of EV_{CRC}, CEA, and CA19-9 were measured at two time points (i.e., post-surgery, L_0; and about 6 months thereafter, L_1), and relative level changes (= $L_1/L_0 - 1$) were calculated. Temporal changes of EV_{CRC} was significantly different between recurrent ($n = 4$) and non-recurrent ($n = 7$) groups ($p = 0.0004$, unpaired two-sided *t*-test). Conventional serum markers showed non-significant differences between recurrent and non-recurrent groups (CEA, $p = 0.13$, unpaired two-sided *t*-test; CA19-9, $p = 0.76$, unpaired two-sided *t*-test). The bar graphs show mean ± SEM.

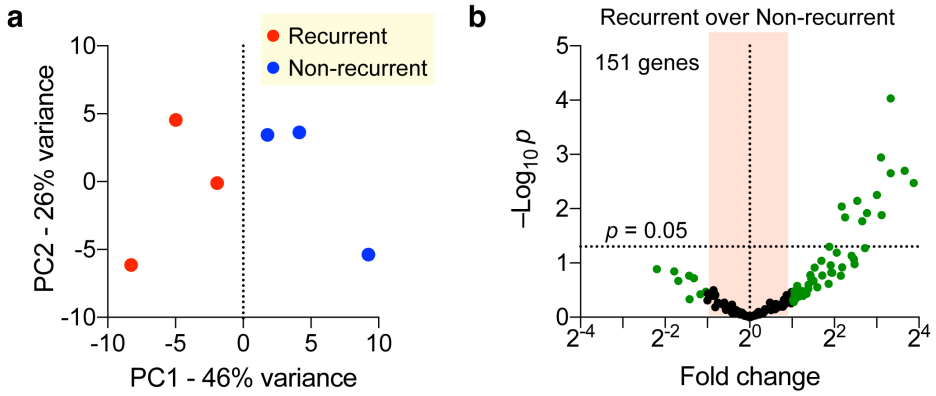

Figure S19 l EV mRNA analyses. EVs were enriched from recurrent ($n = 3$) and non-recurrent ($n = 3$) CRC patients after the completion of adjuvant chemotherapy. EV RNAs were extracted and subjected to targeted mRNA sequencing. Total 370 genes (Human molecular toxicology transcriptome panel, Qiagen) were analyzed and 151 genes were detected. **(a)** Principal component (PC) analysis revealed the separation between recurrent and non-recurrent patient groups. **(b)** RNA expressions were compared between recurrent and non-recurrent patients (two-sided Wald test). More mRNAs were over-expressed in patients with tumor relapse after chemotherapy.

a

Stage	Metastasis	
	– (%)	+ (%)
I	9 (16)	0 (0)
II	24 (43)	5 (15)
III	22 (39)	15 (44)
IV	1 (2)	14 (41)
Total	56 (100)	34 (100)

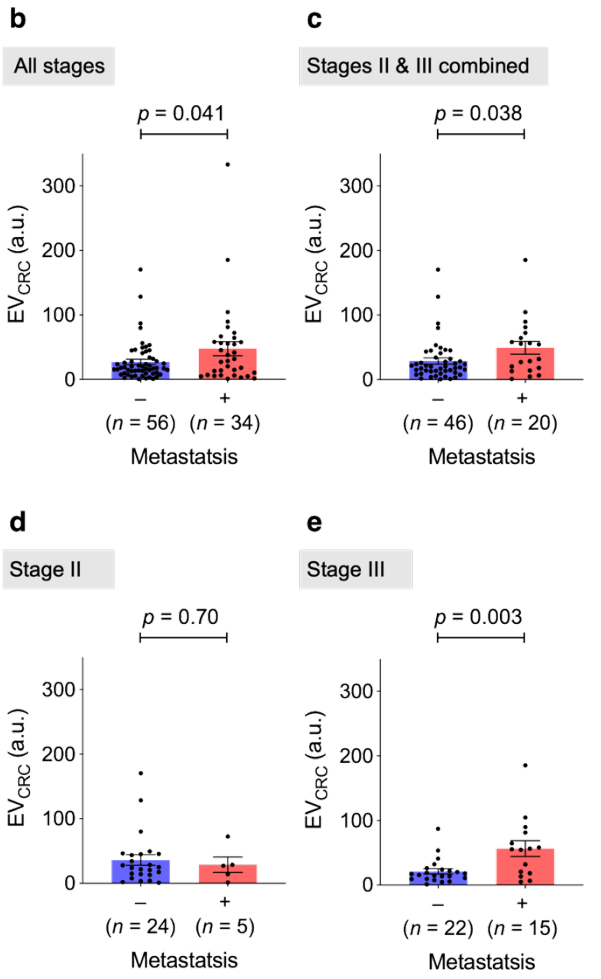

Figure S20 I Preoperative EV_{CRC} levels stratified by metastasis status. (a) Ninety CRC patients were followed up to 61 months after surgery. Fifty six patients (62%) were metastases free, whereas metastatic tumor was found in 34 patients (38%). **(b)** For all stages, the initial EV_{CRC} level was found to be significantly different ($p = 0.041$; unpaired two-sided *t*-test) in the metastatic subgroup. The data were displayed as mean ± SEM. **(c, d, e)** Stage II and III patients were combined (c) or separately (d, e) analyzed. Stage III patient group showed a stronger EV_{CRC} difference per metastasis status. Statistical comparisons were based on unpaired two-sided *t*-test. The data were displayed as mean ± SEM.

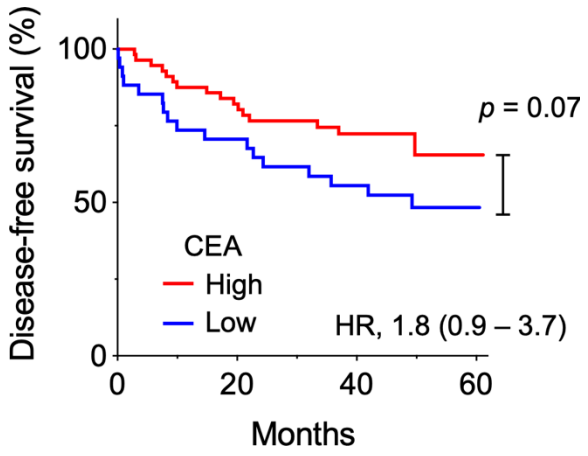

Figure S21 l Survival analyses. DFS for all 90 CRC patients was estimated, stratified by preoperative CEA levels. The conventional cutoff (7 ng/mL) was applied for patient stratification. The survival curves were not significantly different ($p = 0.07$, two-sided log-rank test), and the lower limit of the 95% confidence interval of hazard ration (HR) was < 1.

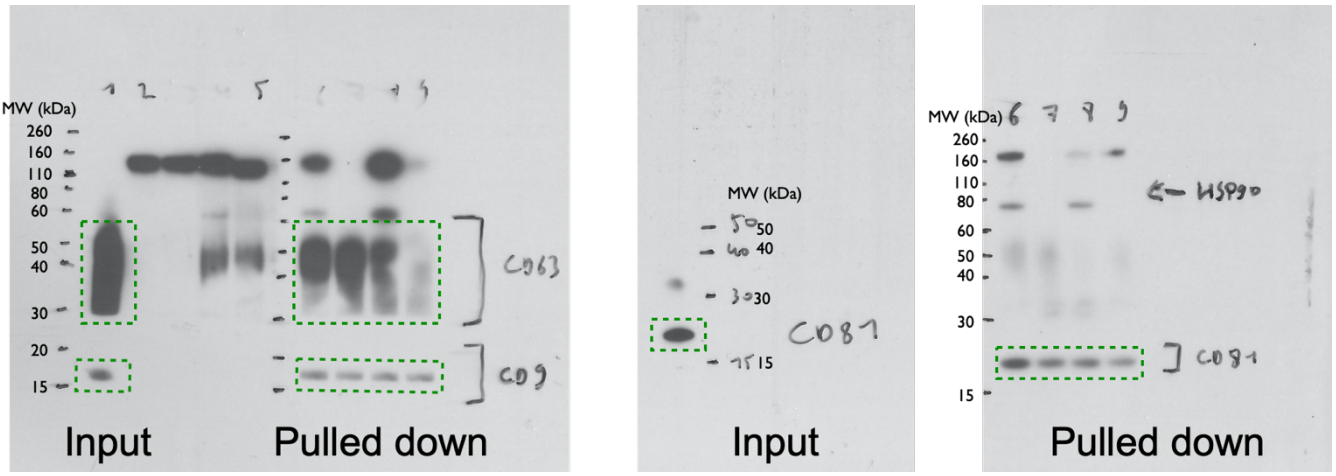

Figure S22 | Original western blot images. The green dashed boxes indicate cropping boundaries. All the films are exposed in one cassette and developed at the same time. Data are selected from technical duplicates.

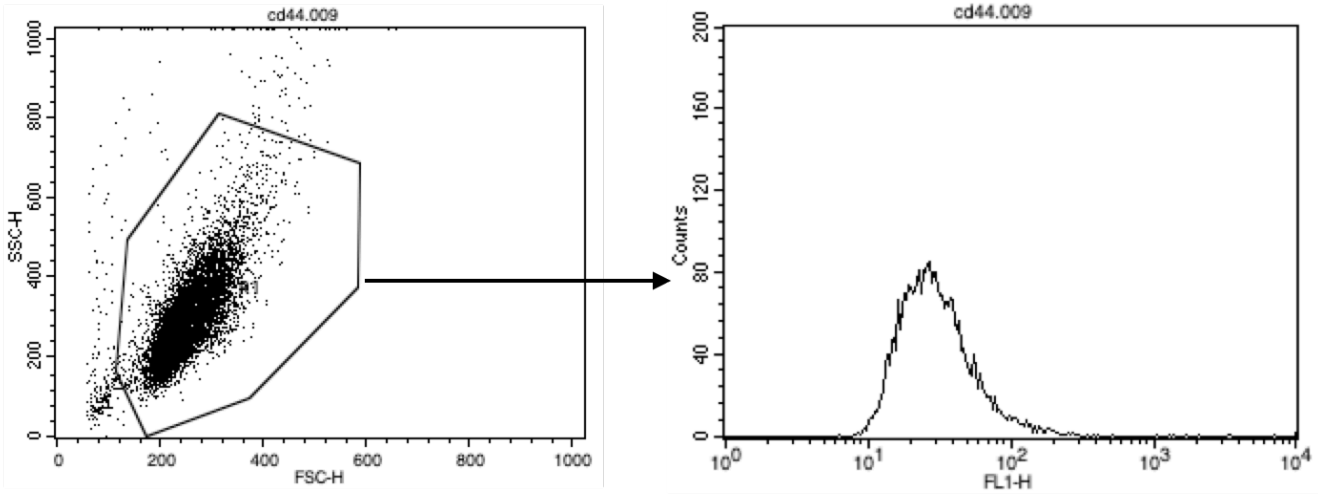

Figure S23 l Flow cytometry gating process. Main population of cells were gated in FCS vs SSC plot. Immuno-fluorescently labeled cells were detected through the FL1 channel. Mean fluorescence intensity were used for data analysis.

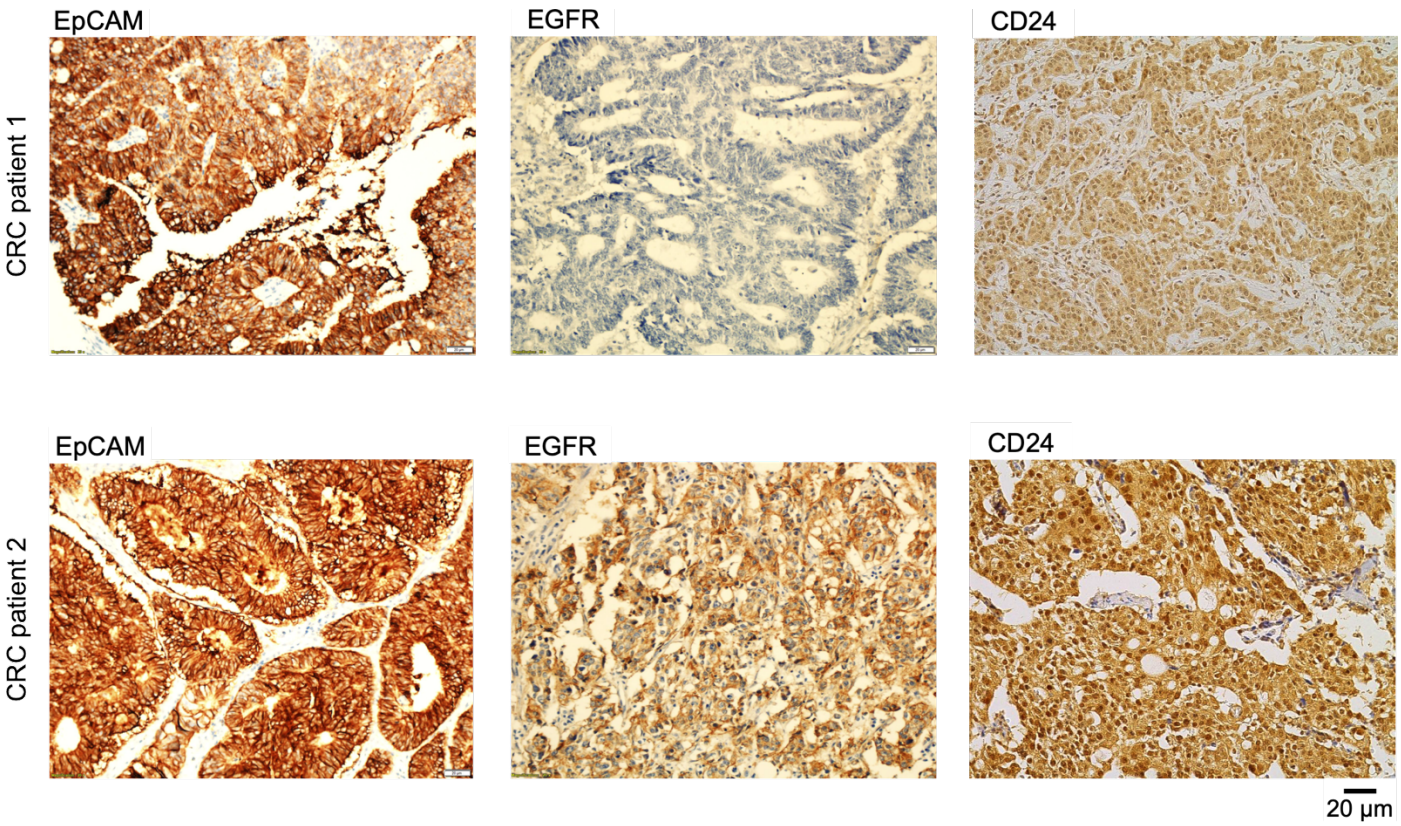

Figure S24 l Full images of stained tissues in Fig. 3a.

Table S1. List of protein markers and their antibodies used in the profiling.

Target	Vendor	Origin	Type
CD63	Ancell (215-020)	Mouse	IgG1,k
CD81	BD (555675)	Mouse	IgG1,k
CD9	BD (555370)	Mouse	IgG1,k
ABCC1	Biolegend (370102)	Mouse	IgG1,k
CD24	ebioscience (eBioSN3)	Mouse	IgG1,k
CD166	Biolegend 343902	Mouse	IgG1,k
EpCAM	AbCAM (VU-1D9)	Mouse	IgG1,k
HER2	Biolegend (24D2)	Mouse	IgG1,k
MET	Abcam (4AT44, ab59884)	Mouse	IgG1,k
Thymidylate synthase	Abcam (TS106, ab3145)	Mouse	IgG1,k
ABCG2	Biolegend (332020)	Mouse	IgG2b, K
CD44v6	R&D (2F10)	Mouse	IgG1,k
CEA	Biolegend (342302)	Mouse	IgG2b, K
EGFR	Abcam (EGFR1)	Mouse	IgG2b, K
MUC1	Fitzgerald (10-M93A)	Mouse	IgG1,k
B7-H3	R&D (185504)	Mouse	IgG1,k
ALDH1	Abcam (ab23375)	Rabbit	polyclonal
CD44	Biolegend (IM7)	Rat	IgG2b, K
CD133	Thermo (PA5-38014)	Rabbit	polyclonal
STEAP1	Thermo (PA5-20404)	Rabbit	polyclonal
MDR1	Biolegend (348602)	Mouse	IgG2a, K
GPA33	Sigmaaldrich (HPA018858)	Rabbit	polyclonal
IgG1	Biolegend (MOPC-21)	Mouse	IgG1,k
IgG2b	Abcam (ab18541)	Rat	IgG2b, K
IgG2a	R&D (133304)	Mouse	IgG2a, K
Rabbit IgG	Biolegend (910801)	Rabbit	polyclonal

Table S2. Clinical information on patient samples used in treatment monitoring.

	Recurrent patients		Non-recurrent patients	
Chemotherapy (FOLFOX)	Yes	No	Yes	No
	4	3	4	0
Age				
Median	53	77	64	-
Range	34–58	54–79	59–67	-
Sex				
Male	3	3	3	-
Female	1	-	1	-
Stage				
I	-	-	-	-
II	-	3	1	-
III	4	-	3	-
IV	-	-	-	-

Table S3. Clinical information on patient samples used for survival monitoring.

	Progression free	Progressed
Number	56	34
Mean DFS months	48.4 (16.1–61.3)	18.0 (0.1–49.7)
Age		
Median	65	70
Range	38–82	34–80
Sex		
Male	33 (59%)	20 (59%)
Female	23 (41%)	14 (41%)
Stage		
I	9 (16%)	0 (0%)
II	24 (43%)	5 (15%)
III	22 (39%)	15 (44%)
IV	1 (2%)	14 (41%)

Table S4. List of antibodies used in Western Blot.

Target	Vendor	Origin	Type
CD63	BD (557305)	Mouse	IgG1,k
CD81	Thermo (MA5-13548)	Mouse	IgG1,k
CD9	Cell signaling (13174)	Rabbit	Monoclonal